
DCAT: DUAL CROSS-ATTENTION FUSION FOR DISEASE CLASSIFICATION IN RADIOLOGICAL IMAGES WITH UNCERTAINTY ESTIMATION

Jutika Borah¹ and Hidam Kumarjit Singh¹

¹Gauhati University, Guwahati 781014, India
borah_jutika@gauhati.ac.in

ABSTRACT

Accurate and reliable image classification is crucial in radiology, where diagnostic decisions significantly impact patient outcomes. Conventional deep learning models tend to produce overconfident predictions despite underlying uncertainties, potentially leading to misdiagnoses. Attention mechanisms have emerged as powerful tools in deep learning, enabling models to focus on relevant parts of the input data. Combined with feature fusion, they can be effective in addressing uncertainty challenges. Cross-attention has become increasingly important in medical image analysis for capturing dependencies across features and modalities. This paper proposes a novel dual cross-attention fusion model for medical image analysis by addressing key challenges in feature integration and interpretability. Our approach introduces a bidirectional cross-attention mechanism with refined channel and spatial attention that dynamically fuses feature maps from EfficientNetB4 and ResNet34 leveraging multi-network contextual dependencies. The refined features through channel and spatial attention highlights discriminative patterns crucial for accurate classification. The proposed model achieved AUC of 99.75%, 100%, 99.93% and 98.69% and AUPR of 99.81%, 100%, 99.97%, and 96.36% on Covid-19, Tuberculosis, Pneumonia Chest X-ray images and Retinal OCT images respectively. The entropy values and several high uncertain samples give an interpretable visualization from the model enhancing transparency. By combining multi-scale feature extraction, bidirectional attention and uncertainty estimation, our proposed model strongly impacts medical image analysis.

Keywords deep learning · feature fusion · cross-attention · classification · uncertainty quantification

1 Introduction

Deep learning (DL) has gained significant traction in medical imaging due to its ability to automate feature extraction, enhance training efficiency, and deliver superior performance across tasks such as classification [Affonso et al., 2017, Sahu and Kashyap, 2025, Mohanty et al., 2024, Thiranjaya et al., 2024], segmentation [Wang et al., 2021, Han et al., 2024], image generation [Pezoulas et al., 2024, Lang et al., 2024], object detection [Ragab et al., 2024, Morita et al., 2024] etc. In particular, automated disease classification in radiology has emerged as a promising clinical diagnosis and treatment planning tool. However, accurate classification remains critical, as errors can lead to misdiagnosis, delayed treatment, or unnecessary interventions. Despite its successes, DL-based lung disorder detection faces notable challenges, including false positives, false negatives, and the complexity of radiological images, which often contain overlapping abnormalities, subtle disease patterns, and intricate anatomical structures [Wang et al., 2017, Rajpurkar et al., 2017]. Standard Convolutional Neural Networks (CNNs) often fall short in addressing these challenges due to their limited ability to capture global context, dynamically prioritize multi-scale features, and integrate contextual relationships crucial for accurate diagnosis [Wang et al., 2020, Lin et al., 2017, Ramamurthy et al., 2024]. Attention mechanisms have emerged as a powerful tool in DL, enabling models to dynamically prioritize the most informative features for a given input,

enhancing adaptability to variations in data distributions. By focusing on less affected features by distribution shifts, attention mechanisms improve model robustness and generalizability across diverse domains [Oktay et al., 2018, Liu et al., 2024].

Additionally, attention weights can offer interpretable insights into the model’s confidence and decision-making process, contributing to more calibrated predictions. In medical image analysis, where data variability and complexity are significant challenges, attention-based feature fusion proves particularly advantageous [Hou et al., 2021, Zheng et al., 2023]. Recent studies, [Valanarasu et al., 2021, Li et al., 2022, Jiang et al., 2021], have explored transformer-based approaches, yet self-attention mechanisms often struggle to capture fine-grained local features, leading to difficulties in distinguishing objects of interest from complex backgrounds. Cross-attention feature fusion addresses this limitation by explicitly modeling relationships between different networks or modalities or views, enabling the model to leverage contextual information from one source to enhance the processing of another [Ates et al., 2023, Song et al., 2022, Zheng et al., 2023]. Unlike traditional fusion methods like concatenation or element-wise addition, cross-attention captures complex dependencies and dynamically weights contributions from each modality, resulting in more informative and nuanced representations. This capability has been demonstrated to improve performance in multi-model and multi-view task significantly [Wang et al., 2023a, Liu et al., 2024], making cross-attention a promising technique for advancing medical image analysis and other complex visual recognition challenges.

Interpretability and uncertainty quantification (UQ) are pivotal challenges [Tjoa and Guan, 2020, Begoli et al., 2019] in the application of DL models to radiology image classification [Faghani et al., 2023, Huang et al., 2024]. The inherent complexity of these models often limits transparency, making it difficult for clinicians to understand how decisions are made. This is particularly problematic in radiology, where high inter-patient variability, differences in imaging protocols, and noise can lead to inconsistent classification outcomes. Moreover, traditional classification networks frequently fail to provide uncertainty estimates, resulting in overconfident misclassifications undermining their reliability in clinical practice. So, quantifying uncertainty is essential for assessing the confidence of model predictions, enabling radiologists to weigh the risks and benefits of diagnostic decisions.

In medical image analysis, recent advancements, such as Medical Transformer [Valanarasu et al., 2021], GasHis Transformer [Chen et al., 2022], and TransFuse [Zhang et al., 2021] have demonstrated the efficacy of combining CNNs with Transformers to capture both global and local features, thereby enhancing performance in tasks like disease detection and segmentation. These approaches emphasize the simultaneous learning of local spatial structures and long-range dependencies to reduce noise and improve feature representation. In contrast, our work introduces a novel Dual Cross-Attention (DCAT) fusion mechanism with enhanced Convolution Block Attention Module (CBAM). By integrating cross-attention between EfficientNetB4 and ResNet34 architectures, our model effectively captures multi-scale features, preserving low-level spatial textures and high-level semantic representations. This approach leverages attention-guided multi-scale global-local fusion to enhance feature representation and address challenges in medical image classification. We incorporate MC Dropout during inference to improve robustness and quantify prediction uncertainty. Validated on four medical image datasets, our proposed DCAT fusion model demonstrates superior performance in lung disease classification from chest X-ray images, and retinal disease classification from OCT images.

1.1 Contribution

The work proposes a new, simple, effective DL model considering its uncertainty for medical image classification.

1. We introduce a cross-attention mechanism that dynamically fuses feature maps from two efficient networks, EfficientNetB4 and ResNet34. DCAT leverages the strength of both the architectures, a bidirectional feature exchange significantly improving feature representation for accurate medical image classification.
2. The integration of channel and spatial attention mechanism refines feature selection. Combining hierarchical cross-attention fusion with enhanced CBAM, captures fine-grained details and high-level semantic information.
3. Incorporating uncertainty quantification provides confidence estimates for each prediction demonstrating the reliability with uncertainty measures for enhancing trustworthiness in clinical decision-making.

The remaining paper follows the given hierarchy: the related works, conventional CNN-based and transformer-based approaches, Attention Mechanism & Feature Fusion, and employed uncertainty quantification are discussed in Section 2, while the proposed model details are provided in Section 3. The details on experiments are provided

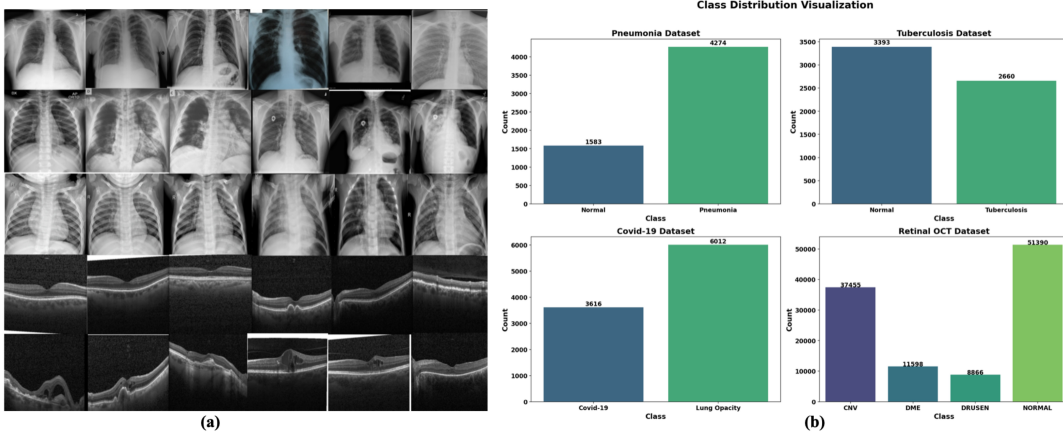


Figure 1: (a) Random example images from the four datasets. From top Tuberculosis chest X-ray, Covid Chest X-ray, Pneumonia Chest X-ray, Retinal OCT images, (b) Visualization of class distribution for each dataset.

in Section 4 followed by experimental result and analysis in Section 5 along with the in-depth discussion of attained results are presented in Section 6. Finally, the conclusion and future work are mentioned in Section 7.

2 Related work

Deep Learning in Radiology. A wide variety of DL models have shown promising outcomes in complicated diagnostic areas across radiology [Borah et al., 2024a, Fritz et al., 2023, Borah et al., 2023], pathology [Ahmed et al., 2022, Unger and Kather, 2024], ophthalmology Jin and Ye [2022], Kazi [2024], Borah et al. [2024b], dermatology, and so on. CNN has been the cornerstone of medical image analysis due to their ability to capture spatial hierarchies in data. Transformer models, introduced by Ashish [2017], have revolutionized the field by effectively handling long-range dependencies through self-attention mechanisms. Models like TransUNet [Chen et al., 2024] and EG-UNETR [Cheng et al., 2024] combine Transformers with CNNs to capture global semantic information while preserving local details. However, Transformer-based models often struggle with computational efficiency and memory constraints, particularly when processing high-resolution medical images and when there is a shortage of data. Additionally, they may fail to preserve fine-grained details, limiting their effectiveness in tasks requiring precise localization. Hybrid models that integrate CNNs and Transformers have emerged as a promising solution, leveraging the strengths of both architectures. However, the computational inefficiency of Transformer-based models and their limited ability to preserve fine-grained details hinder their practical application.

Attention Mechanism & Feature Fusion. Attention mechanisms have emerged as a powerful tool in computer vision. Attention mechanisms can be broadly categorized into channel attention, spatial attention, and cross attention, each addressing specific aspects of feature representation. Channel attention mechanisms, such as Squeeze-and-Excitation (SE) networks [Hu et al., 2018] and selective kernel attention [Chen et al., 2017] allow models to recalibrate channel-wise feature responses, emphasizing important features adaptively. Spatial attention mechanisms, on the other hand, focus on identifying salient spatial regions within feature maps [Woo et al., 2018, Dai et al., 2017]. Techniques like CBAM [Woo et al., 2018] and deformable convolution [Dai et al., 2017] have significantly improved tasks requiring precise localization, such as object detection and segmentation. Self-attention mechanisms, popularized by Transformers [Zhao et al., 2020], capture global dependencies by computing attention weights across all spatial positions [Wang et al., 2023b]. Variants like Swin Transformers [Liu et al., 2021], Focal Transformers [Yang et al., 2021], and HRFormer [Yuan et al., 2021] have extended this capability to process multi-scale information effectively. However, these approaches often neglect to adjust channel dimensions, restricting their capacity to fully leverage channel-wise feature interactions. Cross-attention mechanisms have gained traction for their ability to model relationships between modalities or feature maps. Unlike self-attention, which operates within a single feature space, cross-attention enables exchange between distinct feature representations, enhancing the model’s ability to capture contextual dependencies. For instance, [Schlemper et al., 2019] introduced an attention gate model for medical image analysis, which suppresses irrelevant regions while highlighting task-specific features. Similarly, [Guan et al., 2020] proposed a three-branch attention-

guided CNN for thorax disease identification, integrating global and local cues to improve performance. These studies underscore the potential of attention mechanisms in addressing challenges such as noise suppression and feature refinement. Despite advancements in attention mechanisms, several limitations persist, particularly in cross-attention multi-network feature fusion. While channel and spatial attention mechanisms have been studied extensively, their integration with cross-attention remains insufficiently explored. Finally, the lack of uncertainty quantification in attention limits their reliability in critical applications like medical imaging.

Uncertainty Quantification. UQ techniques used in DL have gained significant attention over the last couple of years in medical data analysis [Faghani et al., 2023, Fayjie et al., 2024, Bai et al., 2024]. By identifying uncertain samples, models can flag complex cases for further investigation, enhancing reliability instead of overconfidently making wrong predictions. A review of the recent advancements in uncertainty quantification was presented in [Zou et al., 2023] which covered different approaches and discussed various applications. Moreover, in [Gawlikowski et al., 2023] factors that cause uncertainty are highlighted, including variability in real-world situations, errors in measurement systems, model structure, training data, and unknown data. Uncertainty in DL can be categorized as aleatoric and epistemic uncertainty [Kendall and Gal, 2017]. Aleatoric uncertainty arises from inherent noise within the data while epistemic uncertainty stems from model limitations. Recent studies have explored various UQ techniques to improve model reliability in medical applications. For instance, Monte Carlo (MC) Dropout has been widely adopted for its simplicity and effectiveness. Nair et al. demonstrated its utility in multiple sclerosis detection and segmentation showing improved performance and uncertainty estimation [Nair et al., 2020]. Similarly, in Chagas et al. [2023] applied MC-Dropout and test-time augmentation for classifying membranous nephropathy showing the importance of correlation between prediction variance and accuracy. While UQ has been extensively studied in traditional DL models, its study with attention mechanism lacks explicit uncertainty modeling and remains underexplored. While ensemble learning methods [Dutschmann et al., 2023, Fayjie et al., 2024] have advanced UQ, they are computationally expensive in resource-constrained environments. This gap motivates our work, to choose and integrate MC-Dropout for UQ into our methodology and evaluate DCAT fusion model for enhanced predictive confidence while maintaining reliability.

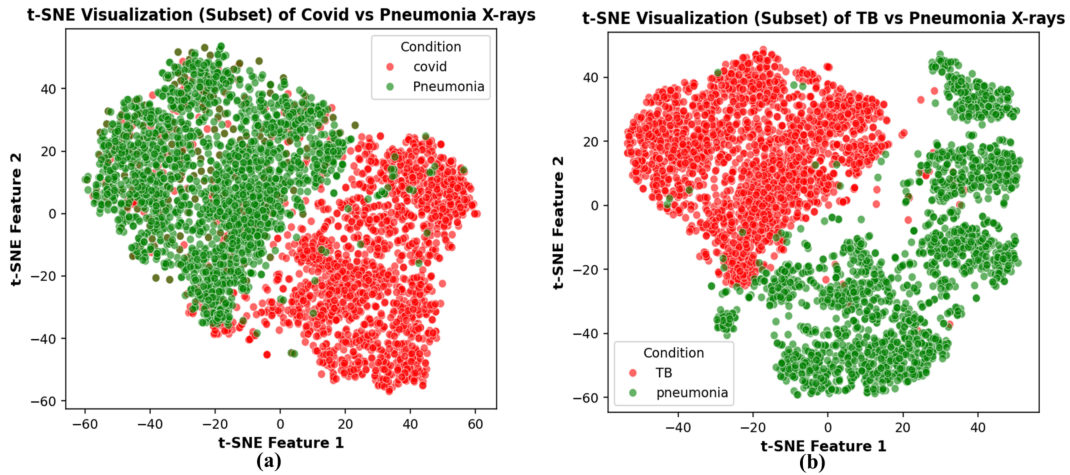


Figure 2: (a) t-SNE plots for visualization and comparison of distributions across datasets to identify similarities (overlap) and differences between (a) Covid-19 original dataset with four classes vs. Pneumonia Chest X-ray dataset, (b) TB vs. Pneumonia Chest X-ray dataset

3 Materials and Methodology

3.1 Materials

In our image classification task, we evaluated the proposed DCAT model using four publicly available medical imaging datasets, Covid-19 chest X-ray [Chowdhury et al., 2020], Tuberculosis chest X-ray [Rahman et al., 2020], Pneumonia Chest X-ray [Kermany, 2018], OCT [Kermany, 2018] images. Figure 1(a) and (b) show some randomly selected samples from four datasets and their class-wise distribution respectively. We randomly split the data into two main sets, where 80% of the data was used for training and the remaining 20% was used as test sets. Two important points to be considered regarding datasets in this work. In the Covid-19 chest X-ray dataset,

the original datasets contain four classes (Covid-19, Lung-Opacity, Viral Pneumonia, and Normal). However, Viral Pneumonia, and Normal classes have similar samples as the Pneumonia chest X-ray datasets. To prevent data leakage and overlapping, we discard these two classes and have considered only the Covid-19 and the Lung Opacity classes from the dataset. The t-SNE plot in Figure 2 (a) and (b) gives the visualization and comparison of distributions across datasets to identify similarities (overlap) and differences.

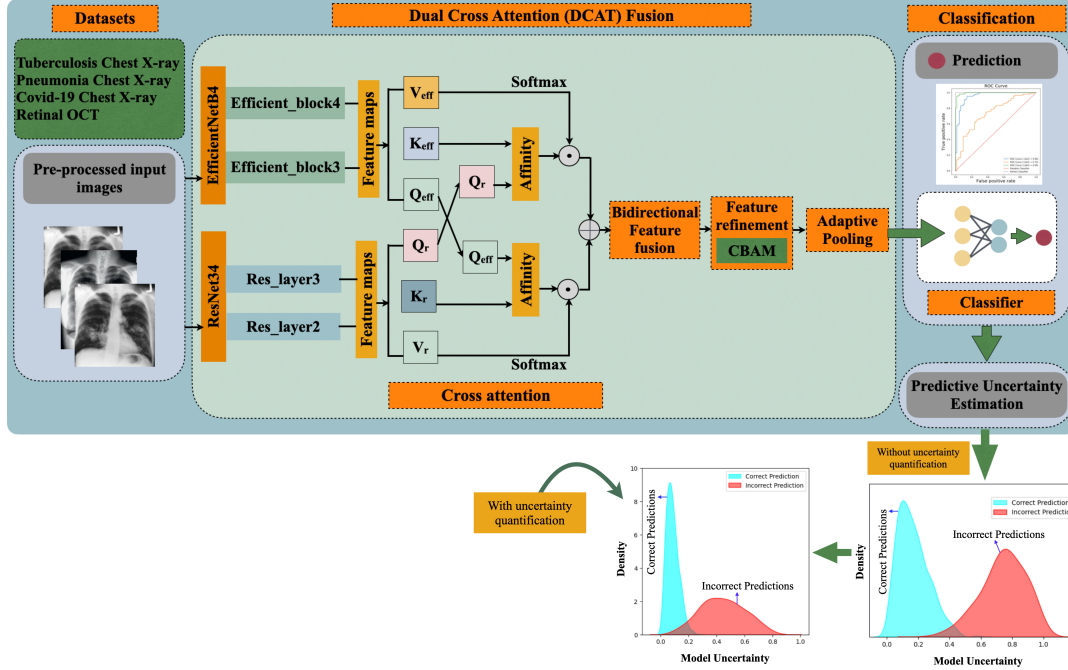


Figure 3: Overview of the proposed DCAT fusion mechanism. The proposed mechanism starts with acquiring chest X-ray and OCT images. The proposed model comprised of local and global feature learning by EfficientNetB4 and ResNet34, cross-attention fusion, and predictive uncertainty estimation. Finally, we have uncertainty estimation quantifying the uncertainty of the model.

3.2 Proposed Methodology

Overview of the Framework This paper proposes a novel cross-attention fusion called the DCAT model that integrates multi-scale feature extraction using EfficientNetB4 and ResNet34 backbones. As illustrated in Figure 3, the proposed architecture comprises four components: dual-branch feature extraction with EfficientNetB4 and ResNet34, hierarchical multi-scale and cross-attention fusion mechanism, refined features using enhanced CBAM attention mechanism, and classification and predictive uncertainty estimation.

EfficientNetB4, part of the Efficient family introduced by Tan and Le [2019] in 2019 employs a compound scaling method that uniformly scales depth, width, and resolution to optimize performance with fewer parameters. This scaling enables the network to capture fine-grained details and high-level semantic information. ResNet34, part of the Residual Network (ResNet) family introduced by He et al. [2016], addresses the vanishing gradient problem through its residual learning framework, enabling the training of deep networks. The architecture extracts hierarchical features, with early layers capturing low-level details and deeper layers capturing high-level semantics. Its residual connections make it robust to over-fitting, even with limited training data. Combining these architectures, the proposed model leverages their complementary strengths in feature representations.

3.3 Feature Extraction

We consider a medical image classification problem where each sample consists of an input image (x) and an associated label $y \in 1, 2, \dots, N_{cl}$, with N_{cl} representing the total number of classes. The feature extraction process is defined using a feature extractor F_{ex} , where $ex \in 1, 2, \dots, N$ denotes the two pretrained feature extractors used in the study. For each pretrained feature extractor, the extracted features are defined as,

$$X_{img}^{ex} = F_{ex}(x)$$

,where X_{img}^{eff} and X_{img}^r represent the feature maps extracted from EfficientNetB4 and ResNet34, respectively. These feature maps capture distinct characteristics of the input image at multiple scales, providing a rich representation for subsequent processing.

3.4 Hierarchical Multi-Scale Feature Extraction

To improve the representation ability of the extracted features, many researchers designed multiple networks to capture more features [Li et al., 2021, Xu et al., 2024]. Huo et al. [2024] constructed a three-branch hierarchical multi-scale feature fusion network that integrates global and local features. In our work, to improve the representation ability of the extracted features, we employ a hierarchical multi-scale feature extraction strategy using EfficientNetB4 and ResNet34. Feature maps extracted from specific layers of these networks are combined to form a multi-scale representation.

The EfficientNetB4 network processes the input image x through a series of Convolutional blocks. Feature maps extracted from EfficientNetB4 Block 3 and 4 have spatial sizes of 28×28 and 14×14 , respectively. Similarly, the ResNet34 network processes the input through a series of residual layers, with feature maps extracted from ResNet Layer 2 and 3 having spatial sizes of 28×28 and 14×14 , respectively. These feature maps are denoted as,

$$\begin{aligned} X_1^{eff} &= \text{EfficientNetB4 Block 3}(x), X_2^{eff} = \text{EfficientNetB4 Block 4}(x) \\ X_1^r &= \text{ResNet34 Layer 2}(x), X_2^r = \text{ResNet34 Layer 3}(x) \end{aligned}$$

The multi-scale feature extraction process produces two sets of concatenated feature maps,

$$F^1 = [X_1^{eff}, X_1^r] \in \mathbb{R}^{2C_1 \times 28 \times 28}, F^2 = [X_2^{eff}, X_2^r] \in \mathbb{R}^{2C_1 \times 14 \times 14}$$

where F^1 represents fine-grained features at a spatial resolution of 28×28 , and F^2 represents high-level features at a spatial resolution of 14×14 . These multi-scale features are then passed to the cross-attention fusion module for further processing.

3.5 Cross Attention mechanism

The attention mechanism computes attention weights for each feature map, identifying its relevance to the classification task. Given an image feature map $F \in \mathbb{R}^{C \times H \times W}$, where C , H , and W denote the number of channels, height, and width of the feature tensor, respectively, our approach employs cross-attention fusion followed by channel and spatial attention modules. Unlike conventional methods, our framework first facilitates feature exchange between EfficientNetB4 and ResNet34 architectures, Figure 3, ensuring that the attention mechanism is guided by multi-network contextual dependencies rather than isolated feature representations. Building on prior works such as [He et al., 2020, Li et al., 2019, Xie et al., 2021], which proposed channel and spatial attention mechanisms to explore discriminative features, our module ensures the network prioritizes disease-specific features by leveraging cross-attention between architectures, enabling context-aware attention refinement. Unlike traditional CBAM [Woo et al., 2018] and SENet [Hu et al., 2018], which apply sequential channel and spatial attention within a single network, our enhanced mechanism integrates cross-network feature interactions. This approach enhances spatial understanding and multi-scale feature integration, addressing the limitations of single-network attention mechanisms.

Let $X_{img}^{eff} \in \mathbb{R}^{C \times H \times W}$ represent the feature map from EfficientNetB4, and $X_{img}^r \in \mathbb{R}^{C \times H \times W}$ represent the feature map from ResNet34. To enable bi-directional attention fusion, we compute Query(Q), Key(K), and Value(V) representations of both networks. For EfficientNetB4, Q termed as Q_{eff} is derived from ResNet34 features and are the transformed EfficientNetB4 features (shown in Figure 3). K and Q termed as K_{eff} and V_{eff} respectively are computed from EfficientNetB4 features.

$$\begin{aligned} &\text{EfficientNetB4} \rightarrow \text{ResNet34} \\ Q_{eff} &= W_q X_{img}^r, K_{eff} = W_k X_{img}^{eff}, V_{eff} = W_v X_{img}^{eff} \end{aligned}$$

For ResNet34, Q termed as Q_r is derived from EfficientNetB4 features and are the transformed ResNet34 features (shown in Figure 3). K and Q , termed as K_r and V_r respectively, are computed from the ResNet34 features.

$$\begin{aligned} &\text{ResNet34} \rightarrow \text{EfficientNetB4} \\ Q_r &= W_q X_{img}^{eff}, K_r = W_k X_{img}^r, V_r = W_v X_{img}^r \end{aligned}$$

Here, W_q , W_k , and W_v are learnable weight matrices that project input features into attention space. The attention weights are computed using the scaled dot-product attention mechanism. For EfficientNetB4 attending to ResNet34, the attention is calculated as,

$$\text{Attention}(Q_{eff}, K_r, V_r) = \text{Softmax} \left(\frac{Q_{eff} K_r^T}{\sqrt{d_k}} \right) V_r \quad (1)$$

where $Q_{eff} K_r^T$ measures the similarity between the queries and keys, and $\sqrt{d_k}$ is a scaling factor that stabilizes gradients. Similarly, for ResNet34 attending to EfficientNetB4, the attention is computed as,

$$\text{Attention}(Q_r, K_{eff}, V_{eff}) = \text{Softmax} \left(\frac{Q_r K_{eff}^T}{\sqrt{d_k}} \right) V_{eff} \quad (2)$$

where $Q_r K_{eff}^T$ measures the similarity between the queries and keys, and $\sqrt{d_k}$ is a scaling factor that stabilizes gradients. The final fused feature map F_{fusion} is obtained by combining the attention outputs from both the directions,

$$F_{fusion} = \text{Attention}(Q_{eff}, K_r, V_r) + \text{Attention}(K_{eff}, Q_r, V_{eff}) \quad (3)$$

This bidirectional fusion ensures that the final feature representation incorporates complementary information from both networks, enhancing the model's ability to capture subtle patterns and relationships in the data.

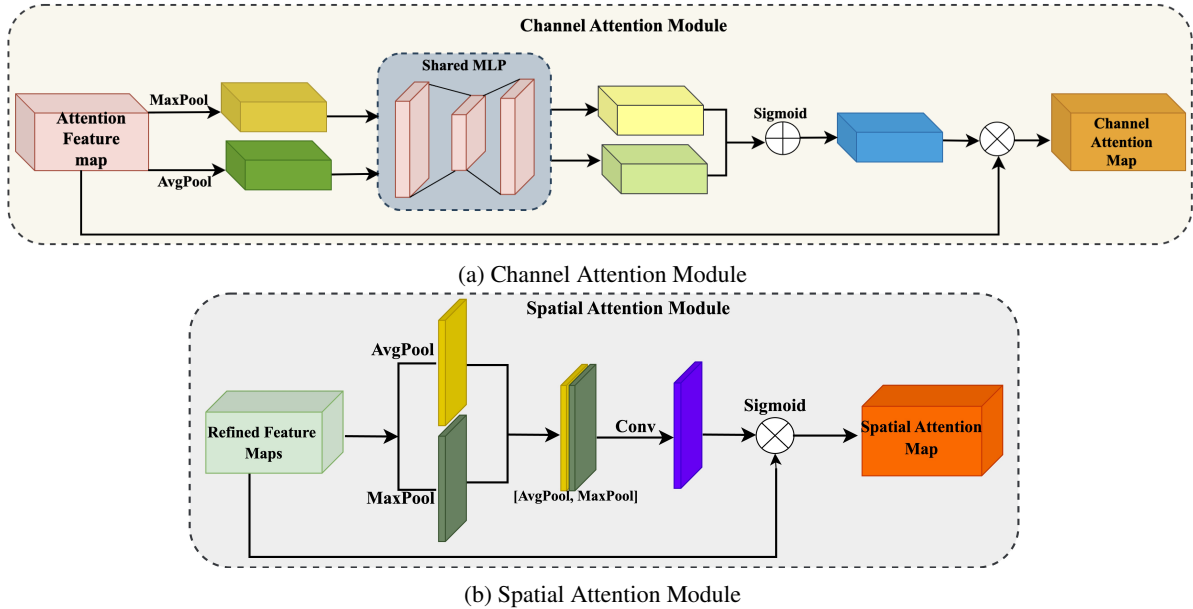


Figure 4: (a) Channel-attention and (b) spatial attention module as part of the CBAM used in this study. The proposed DCAT fuses feature maps from the two pretrained models before applying channel and spatial attention, enabling our proposed model to leverage information from the two networks and enhancing the feature representations for the classification task.

3.6 Feature Refinement and Classification

Following the cross-attention fusion, we refine the feature maps using an enhanced version of the CBAM attention mechanism (Figure 4). By leveraging channel and spatial attention mechanisms, our refined CBAM enables the model to attend to the channel and spatial axes, respectively.

3.6.1 Channel Attention Mechanism.

The channel attention mechanism computes attention weights for each channel in the fused feature map $F_{fusion} \in \mathbb{R}^{C \times H \times W}$ where C , H , and W represent the number of channels, height, and width, respectively. To aggregate spatial information, both average pooling and max pooling are applied to F_{fusion} ,

$$\text{AvgPool}(F_{fusion}) = \frac{1}{H \times W} \sum_{i=1}^H \sum_{j=1}^W F_{fusion}(i, j) \quad (4)$$

$$\text{MaxPool}(F_{fusion}) = \max_{i \in H, j \in W} F_{fusion}(i, j) \quad (5)$$

The pooled features are combined and passed through a shared multi-layer perceptron (MLP) with weights W_1 and W_2 , followed by ReLU activation and a sigmoid function (σ),

$$M_c = \sigma(W_2 \text{ReLU}(W_1 (\text{AvgPool}(F_{fusion}) + \text{MaxPool}(F_{fusion})))) \quad (6)$$

Here, $M_c \in \mathbb{R}^{C \times 1 \times 1}$ represents the channel attention weights, which highlight the most important channels. The refined feature map $F_{refined}$ is obtained by multiplying M_c with F_{fusion} .

3.6.2 Spatial Attention Mechanism.

The spatial attention mechanism computes attention weights for each spatial location in the feature maps. Both average pooling and max pooling are applied along the channel dimension, and the results are concatenated. A convolutional layer with weights W_s is applied, followed by a sigmoid function,

$$M_s = \sigma(W_s \times [\text{AvgPool}(F_{fusion}), \text{MaxPool}(F_{fusion})]) \quad (7)$$

Here, $M_s \in \mathbb{R}^{1 \times H \times W}$ represents the spatial attention weights. The final refined feature map is obtained by applying both channel and spatial attention mechanisms. This joint refinement process ensures that important channels and spatial regions are emphasized, enhancing the discriminative power of the feature. This approach significantly improves feature representation, making it particularly effective for medical image analysis tasks.

3.6.3 Feature pooling and classification.

The refined feature maps $F_{refined} \in \mathbb{R}^{C \times H \times W}$ are passed through an adaptive average pooling layer to reduce their spatial dimensions to a fixed size, ensuring compatibility with the fully connected layer regardless of the input image size,

$$F_{pooled} = \text{AdaptiveAvgPool}(F_{refined}) \quad (8)$$

where $F_{refined} \in \mathbb{R}^{C \times 1 \times 1}$ represents the pooled feature map. The pooled features are then flattened into a vector and passed through a fully connected layer with weights W_c and bias b ,

$$y = \text{Softmax}(W_c F_{pooled} + b) \quad (9)$$

Here, y represents the output probability distribution over the possible class labels. The sigmoid activation function ensures that the output values sum to one, providing a probabilistic interpretation of the model's predictions. The class with the highest probability is selected as the predicted label \hat{y} .

3.7 Model Uncertainty Calculation.

MC-Dropout. A widely used technique for quantifying uncertainty and introduced by Gal and Ghahramani [Gal and Ghahramani, 2016], this method treats dropout regularization as a Bayesian approximation, enabling scalable learning of predictive distributions. Traditionally, dropout is applied during training to prevent over-fitting by randomly deactivating neurons, which reduces reliance on specific training data patterns. MC Dropout extends this concept by activating dropout during training and testing. This approach involves running multiple stochastic

forward passes on the same input, effectively generating a predictive distribution. The resulting softmax outputs are averaged to form the final prediction while also reflecting the model’s uncertainty.

Consider a trained network model, $f_{\theta}(\cdot)$ where f is the network and θ is the learnable parameters with an active dropout. Suppose a new test x, y is to be predicted, where x is the array of images and y is the corresponding label. It will be passed through the network with active dropout M times (i.e. no. of forward passes). Thus, the predictive posterior distribution can be approximated to generate the final prediction as follows:

$$p(y|x) = \frac{1}{M} \sum_{m=1}^M p_m \quad (10)$$

where p_m denotes the output of the softmax function at pass $m \in 1, \dots, M$.

$$p_m = \text{Softmax}(f_{\theta_m}(x)) \quad (11)$$

Following the work of [Gal and Ghahramani, 2016], we enable the dropouts during inference. Our experiment computes the posterior probability distribution over the trained network weights given the input sample and the corresponding ground truth. 100 forward passes are performed to quantify uncertainty, and an average is taken to produce the final prediction. We used a dropout with a rate of 0.5 during training.

4 Experiments

4.1 Implementation details

We choose Pneumonia, Covid-19, Tuberculosis, and Normal for chest X-ray images belonging to three different datasets and CNV, DME, DRUSEN, and Normal for retinal OCT images as the categories of classification task. Our chest X-ray images are collected from public repositories. We implement the proposed mechanism and perform experiments using the PyTorch library. Training and evaluations have been accomplished using NVIDIA GeForce RTX 3060 Ti inbuilt GPU. The batch size for training is set to 32. The maximum epochs is set to 200 and the learning rate is initialized to $3e - 4$ with a weight decay of $1e - 4$. We choose Adam as the optimizer for the training stage. The whole training process takes 2h30min and the testing time for a per radiology image is approximately 0.015s.

4.1.1 Evaluation metrics

For a comprehensive overview and evaluation of the performance of the proposed model, we employed standard performance metrics like accuracy, AUC is the area under the ROC curve (AUROC), Area Under the Precision-Recall (AUPR), precision, recall, specificity, F1-score, Matthews Correlation Coefficient (MCC) and Cohen’s Kappa. As our dataset is class-imbalanced, we use the AUPR as a metric that evaluates classification performance. AUC, AUPR focus on positive class performance. MCC and Cohen’s Kappa are both metrics used to evaluate classification performance, but they have distinct differences in handling agreement and correlation. Since our datasets are class imbalanced, we considered MCC for evaluating the classifier performance. The Kappa coefficient, is used to measure the classification accuracy of the model and can also be used for consistency testing.

$$\text{Accuracy} = \frac{TP + TN}{TP + FP + TN + FN} \quad (12)$$

$$\text{Precision} = \frac{TP}{TP + FP} \quad (13)$$

$$\text{Recall} = \frac{TP}{TP + FN} \quad (14)$$

$$\text{Specificity} = \frac{TN}{TN + FP} \quad (15)$$

$$\text{F1_score} = \frac{2 \times \text{Precision} \times \text{Recall}}{\text{Precision} + \text{Recall}} \quad (16)$$

$$\text{MCC} = \frac{TP \times TN - FP \times FN}{\sqrt{(TP + TN)(TP + FN)(TN + FP)(TN + FN)}} \quad (17)$$

$$\text{Kappa} = \frac{p_0 - p_e}{1 - p_e} \quad (18)$$

Here, TN , TP , FN , FP are true negative, true positive, false negative and false positive respectively. In Cohen Kappa, p_0 , and p_e represent observed agreement, and expected agreement by chance.

4.1.2 Uncertainty evaluation metrics

Entropy. Entropy is directly related to the confidence of a model’s prediction. When entropy is high, it signals that the model is uncertain and that it might benefit from additional information and vice versa. It’s a measure of variability associated with random variables [Shannon, 1948]. Entropy facilitates transparency by quantifying uncertainty, making it easier for clinicians to make informed decisions. Since medical imaging deals with complex, noisy, and ambiguous data, images like X-rays can have varying levels of quality and precision. In the context of predictive uncertainty, entropy measures the uncertainty of a probability distribution over possible outcomes and is defined mathematically as -

$$H(p(y|x)) = - \sum_{c=1}^C p(y|x) \log p(y|x), \quad (19)$$

Here, C is the number of classes.

Table 1: Performance comparison of our proposed DCAT applied to four datasets at evaluation stage with uncertainty quantification. HUS → High Uncertainty Sample

Datasets	Accuracy	Mean Entropy	Standard deviation	HUS	Misclassified Samples
Covid-19	97.41	0.0254	0.1011	3	12
Tuberculosis	99.21	0.0024	0.0353	7	10
Pneumonia	98.95	0.0150	0.0817	5	11
OCT	91.17	0.1603	0.2457	45	36

Table 2: Details of class-wise classification performance of four datasets used in this study. CNV → Choroidal neovascularization, DME → Diabetic Macular Edema

Datasets	Classes	Precision	Recall	Specificity	F1-score
Covid-19 Chest X-ray	Covid-19	94.63	98.17	98.17	96.37
	Lung Opacity	98.86	96.60	96.53	97.72
Pneumonia Chest X-ray	Pneumonia	98.29	98.55	98.63	98.42
	Normal	96.14	95.47	95.43	95.80
Tuberculosis Chest X-ray	Tuberculosis	99.21	94.74	94.74	96.92
	Normal	96.02	99.41	99.41	97.68
Retinal OCT	CNV	92.90	90.04	97.39	91.45
	DME	96.13	91.24	98.80	93.62
	DRUSEN	88.59	83.87	96.98	86.16
	NORMAL	87.44	98.43	95.04	92.61

5 Experimental Results and Analysis

A comprehensive assessment of the proposed model’s performance was conducted and the findings are reported through performance metrics in the subsequent tables. To evaluate the effectiveness of the proposed model from different perspectives, we experimented on four different medical imaging datasets as listed in the earlier section. The experimental results of the four datasets are shown in Table 1, 2 and 3 respectively. The results from our ablation study are shown in Table 4, effectively demonstrating the performance of various individual components

within the DCAT on classification performance. We also evaluated the performance with some of the already published works.

As shown in Table 5, demonstrates the effectiveness of our DCAT model. Our proposed model achieved accuracy of 97.41%, 99.21%, 98.95%, and 91.17% for Covid-19 chest X-ray, tuberculosis chest X-ray, pneumonia chest X-ray, and retinal OCT datasets, respectively. The AUROC and PR-curves of the proposed DCAT are shown in Figures 5, for the three chest X-ray datasets, and the retinal OCT dataset respectively.

Table 3: Performance comparison of our proposed DCAT applied to various chest X-ray and retinal OCT images at evaluation stage

Datasets	AUC	AUPR	Precision	Recall	Specificity	F1-Score	MCC	kappa
Covid-19	99.75	99.81	98.21	97.35	97.50	97.78	94.68	94.67
Tuberculosis	100.0	100.0	100.0	98.68	100.0	99.34	98.83	98.82
Pneumonia	99.93	99.97	99.21	99.34	97.91	99.27	97.35	97.35
OCT	98.69	96.36	91.33	91.17	97.05	91.13	88.27	88.17

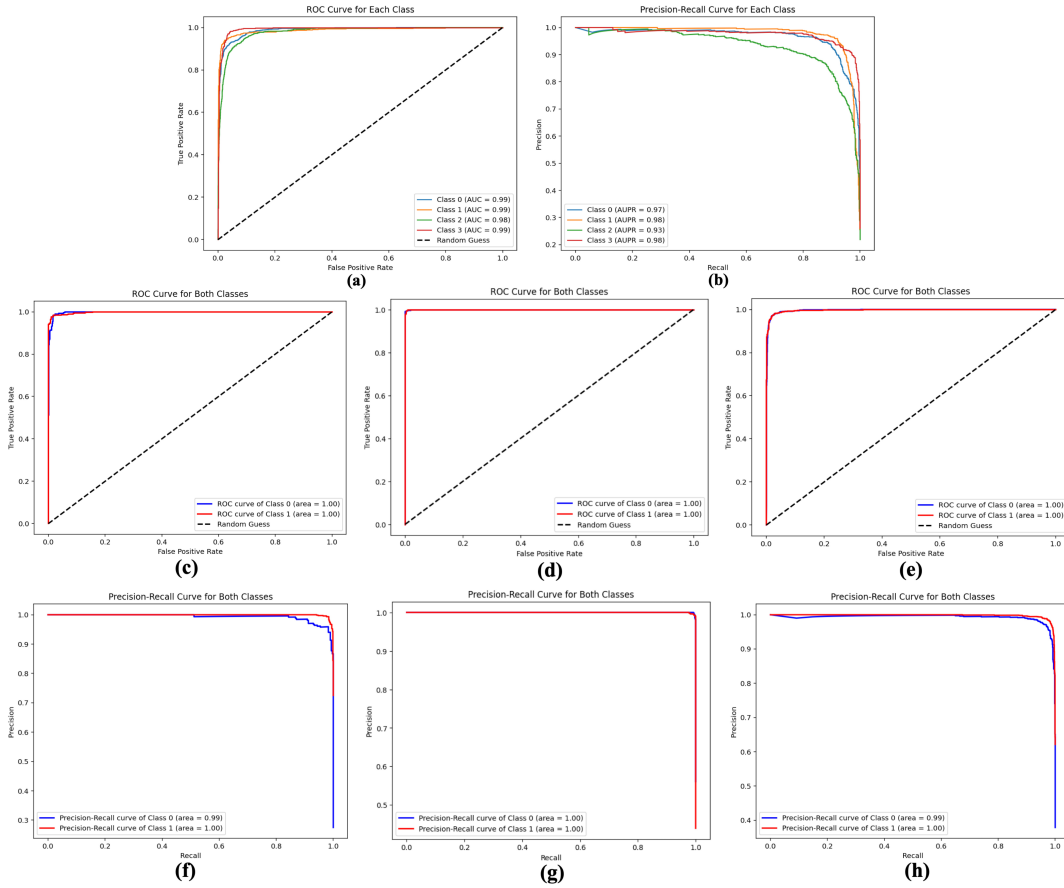


Figure 5: AUROC Curve and Precision-Recall Curve. From the top-left: Retinal OCT (a) AUROC Curve (b) Precision-Recall Curve, Covid-19 Chest X-ray (c) AUROC Curve (f) Precision-Recall Curve, Pneumonia Chest X-ray (d) AUROC Curve (g) Precision-Recall Curve, and Tuberculosis Chest X-ray (e) AUROC (h) Precision-Recall Curve

5.1 Ablation Studies

A comprehensive ablation study was conducted to validate and justify the component of the proposed model on the four datasets and the evaluation metrics previously discussed. The analysis supports our design choices, thereby providing valuable insights into each element's significance in enhancing the performance of the DCAT,

and achieving the desired outcomes. Table 4 summarizes the dataset’s results without DCAT mechanism. This shows that each component of the model contributes to the overall performance. Table 5 compares our proposed DCAT with other recently proposed deep learning methods.

Table 4: Performance comparison of EfficientNetB4 models ResNet34 at individual level without cross attention mechanism on the four datasets

Datasets	ResNet34 ¹			EfficientNetB4 ²		
	Accuracy	Entropy	Standard deviation	Accuracy	Entropy	Standard deviation
Covid-19	86.99	0.0443	0.0239	88.76	0.0926	0.0172
Tuberculosis	80.94	0.1896	0.0948	85.89	0.2000	0.0968
Pneumonia	81.89	0.0500	0.0467	80.77	0.0756	0.0891
OCT	88.91	0.2646	0.0367	90.18	0.1290	0.2567

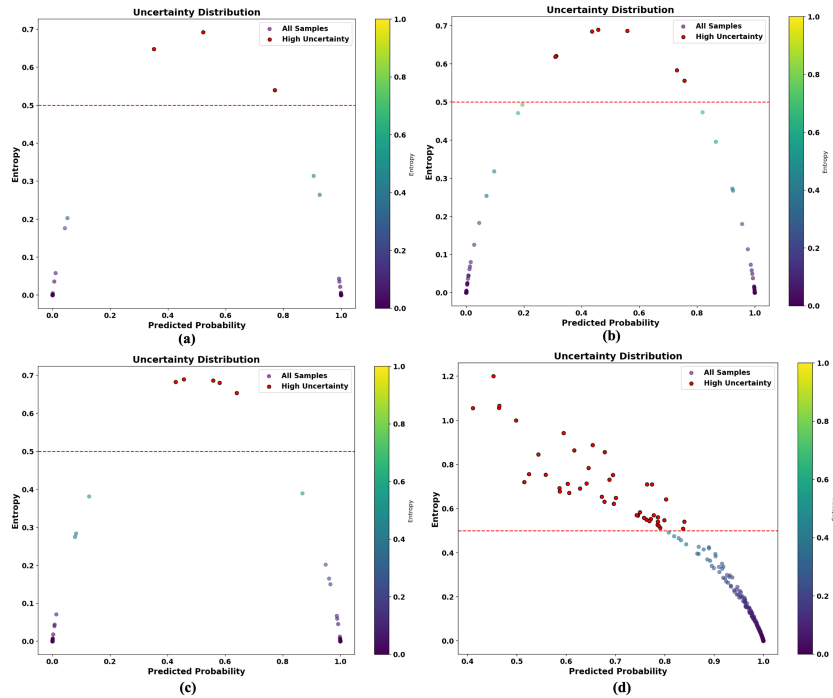


Figure 6: Uncertainty distribution visualization of a subset of data from each dataset with all samples and samples with high uncertainty above an uncertainty threshold. From the left: (a) Covid-19 Chest X-ray, (b) Tuberculosis Chest X-ray, (c) Pneumonia Chest X-ray, and (d) Retinal OCT

Table 5: Performance comparison of various deep learning models and our proposed DCAT fusion model applied to OCT, Pneumonia, Tuberculosis, and Covid-19 datasets at the evaluation stage

Methods	Datasets	Accuracy	AUC	UQ	Mean Entropy	Standard deviation	HUS
Abdar et al. [2021]	Pneumonia	81.57	92.60	Yes	–	–	–
Yang et al. [2023]	Pneumonia	94.60	99.10	No	–	–	–
Chhikara et al. [2020]	Pneumonia	90.70	–	No	–	–	–
DCAT (Ours)	Pneumonia	98.95	99.93	Yes	0.0150	0.0817	13
Abdar et al. [2021]	OCT	91.40	98.21	Yes	–	–	–
Yang et al. [2023]	OCT	77.60	96.20	No.	–	–	–
DCAT (Ours)	OCT	91.17	98.60	Yes	0.1603	0.2457	45

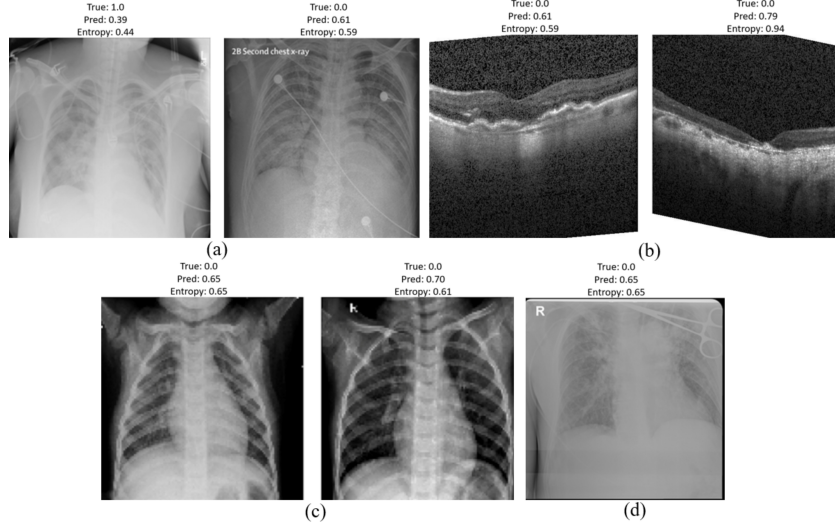


Figure 7: Random high uncertain samples from four datasets with entropy value, predicted probability, and ground-truth. From the left: (a) Covid-19 Chest X-ray, (b) retinal OCT, (c) Pneumonia Chest X-ray, and (d) Tuberculosis Chest X-ray dataset

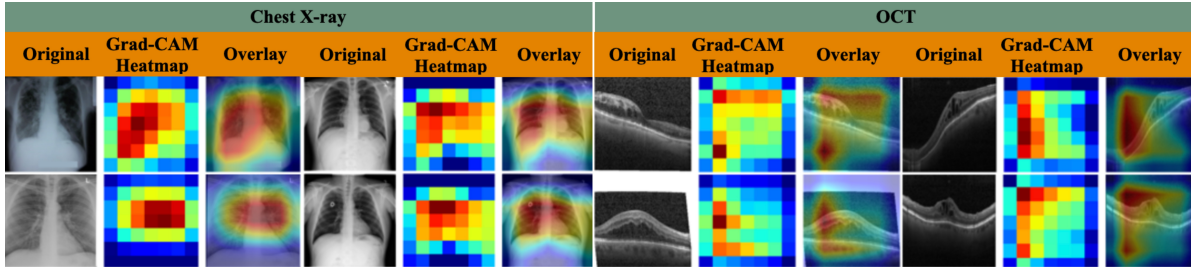


Figure 8: Visualization of Grad-CAM analysis on chest X-ray and OCT datasets using DCAT from the left: Original chest X-ray and OCT images, their corresponding heat maps, and the Grad-CAM overlays and repeating the same towards the right.

6 Discussion

In the last few decades, the impressive performance of DL methods broadly applied to various fields of application, from engineering to healthcare, is a reason for using such methods in analyzing medical data. However, due to insufficient labeled medical datasets, most DL methods rarely achieve the desired performance. In this article, inspired by previous studies, we therefore propose a cross-attention fusion method called DCAT for classification of various medical image datasets. Unlike most previous fusion models, the proposed DCAT fusion model takes the advantage of a new approach called deep hierarchical dual cross-attention fusion, which can separate different classes within the datasets. This can be visualized by the AUPR and MCC values given in Table 3.

We developed a novel hierarchical DCAT fusion model as stated in Figure 3. As indicated, we hierarchically obtain the features from EfficientNetB4, which is our first feature extractor, and then the second feature extractor, ResNet34. Unlike the previous feature fusion, instead of using original features extracted by pretrained models, we proposed a feature fusion based on the cross attention mechanism. An attention mechanism is utilized to detect the relevant features in each stage and then combine them. In addition, as most previous studies did not consider estimating the uncertainty in their model, we included uncertainty estimation in our experimental study. Unlike prior studies applied with feature fusion or cross attention, including simple dropout or performance evaluation on standard metrics, where we do not get enough information on how uncertain and certain the model is in its predictions and its reliability. We overcome this in our proposed work by showing entropy as a metric of uncertainty evaluation and finding the number of total highly uncertain samples to flag them for additional expert investigation and review. This is a critical component for reliability and interoperability in any DL-based systems in safety-critical applications such as medicine and healthcare. We quantify uncertainties during all the stages

of our experimentation. To better reveal the importance and impact of our proposed DCAT, its performance is compared with other methods in Table 5. The visual explanation of the proposed DCAT fusion model using heat map and gradient-weighted class activation mapping (Grad-CAM) techniques is presented in Figure 8. Finally, the probability distribution of the predictions for each class obtained by the proposed DCAT fusion model for four datasets are presented in Table 2, respectively. In Table 1, we show some high uncertainty samples (HUS) and misclassified samples. In Figure 7 we demonstrate high uncertain samples from each dataset based on entropy, ground-truth and predictive probability. These highly uncertain samples can be flagged to the medical experts for further investigation and clarification.

Altogether, the key advantage of using the proposed DCAT is as follows. 1) It considers a hierarchical dual cross attention where each model contributes to the final prediction where it has the advantage of feature fusion by looking closely attending and informing the model what to look at and where to look at, 2) Using uncertainty quantification method to evaluate the prediction of the model and uncertainties during each stages, and number of high uncertain and misclassified samples. 3) Because our datasets are class-imbalanced, the AUC, AUPR and MCC values in Table 3 show that our model is confident in most cases in discriminating between the positive and negative cases while making a few errors.

In medical imaging, translating a diagnosis into clinically actionable information for evaluating the health of a patient, they are guided by their intuitions and knowledge. Here, the reliability will be on the model’s identification and understanding of features that align with medical practice based evidence. Different variations can lead to variations in DL model’s performance, such as specific medical imaging modality, which has its unique challenges, its data availability and tasks, resolution of images, and its preprocessing requirements, information contents, architectural complexity within the model, and clinical variability. So, understanding the requirements and subtle differences in building effective DL solutions. Considerations incorporating such spectrum into the design of model, training, and evaluation would be effective and transferable in clinical applications. Quantifying the uncertainty within model’s predictions offers a more robust and scalable approach to navigating real-world healthcare data complexities. This facilitates in providing a confidence in the interpretation of medical images for clinical decision-making while contributing to the interpretability of the model allowing the clinicians to identify cases that are most uncertain for further investigation and verification. Future work should investigate the implementation of how the uncertainties within the model can be enhanced through building more robust and adaptive models and extending to CT and MRI data.

7 Conclusion

This article proposed a novel, simple, yet effective feature fusion model with uncertainty quantification based on a hierarchical dual cross-attention fusion approach called DCAT considering two pretrained models. The proposed fusion model was validated using three well-known medical chest X-ray and OCT datasets. Our proposed model had successfully captured the spatial relationships between features extracted by two pretrained DL models and obtained high classification performance with the DCAT feature fusion approach. The model generalized the attention mechanism concept as a selective type of feature fusion into the main learning framework. The model yielded high classification performance owing to the hierarchical multi-scale dual feature fusion strategy. We plan to extend our proposed model to the medical image segmentation task and extend the work to enhance the uncertainties within the model for adaptive and robust performance. Future work also includes investigation and extending to pathophysiology, CT, and MRI data.

Declaration of Competing Interest

The authors declare no competing interests or any relationships that could influence the work reported in this paper.

References

- Carlos Affonso, André Luis Debiasio Rossi, Fábio Henrique Antunes Vieira, André Carlos Ponce de Leon Ferreira, et al. Deep learning for biological image classification. *Expert systems with applications*, 85:114–122, 2017.
- Hemlata P Sahu and Ramgopal Kashyap. Fine_denseiganet: Automatic medical image classification in chest ct scan using hybrid deep learning framework. *International Journal of Image and Graphics*, 25(01):2550004, 2025.

- Bipin Ch Mohanty, PK Subudhi, Ratnakar Dash, and Bidyadhar Mohanty. Feature-enhanced deep learning technique with soft attention for mri-based brain tumor classification. *International Journal of Information Technology*, 16(3):1617–1626, 2024.
- Wickramaarachchi Minidu Thiranjaya, Yuan Li, Lei Tao, and Yuemei Luo. Cross-domain retinopathy classification with oct images via disentangling representation and adaptation networks. In *2024 9th Optoelectronics Global Conference (OGC)*, pages 179–183. IEEE, 2024.
- Shanshan Wang, Cheng Li, Rongpin Wang, Zaiyi Liu, Meiyun Wang, Hongna Tan, Yaping Wu, Xinfeng Liu, Hui Sun, Rui Yang, et al. Annotation-efficient deep learning for automatic medical image segmentation. *Nature communications*, 12(1):5915, 2021.
- Kai Han, Victor S Sheng, Yuqing Song, Yi Liu, Chengjian Qiu, Siqi Ma, and Zhe Liu. Deep semi-supervised learning for medical image segmentation: A review. *Expert Systems with Applications*, page 123052, 2024.
- Vasileios C Pezoulas, Dimitrios I Zaridis, Eugenia Mylona, Christos Androustos, Kosmas Apostolidis, Nikolaos S Tachos, and Dimitrios I Fotiadis. Synthetic data generation methods in healthcare: A review on open-source tools and methods. *Computational and structural biotechnology journal*, 2024.
- Oran Lang, Doron Yaya-Stupp, Ilana Traynis, Heather Cole-Lewis, Chloe R Bennett, Courtney R Lyles, Charles Lau, Michal Irani, Christopher Semturs, Dale R Webster, et al. Using generative ai to investigate medical imagery models and datasets. *EBioMedicine*, 102, 2024.
- Mohammed Gamal Ragab, Said Jadid Abdulkader, Amgad Muneer, Alawi Alqushaibi, Ebrahim Hamid Sumiea, Rizwan Qureshi, Safwan Mahmood Al-Selwi, and Hitham Alhussian. A comprehensive systematic review of yolo for medical object detection (2018 to 2023). *IEEE Access*, 2024.
- Daiki Morita, Ayako Kawarazaki, Mazen Soufi, Yoshito Otake, Yoshinobu Sato, and Toshiaki Numajiri. Automatic detection of midfacial fractures in facial bone ct images using deep learning-based object detection models. *Journal of Stomatology, Oral and Maxillofacial Surgery*, page 101914, 2024.
- Xiaosong Wang, Yifan Peng, Le Lu, Zhiyong Lu, Mohammadhadi Bagheri, and Ronald M Summers. Chestx-ray8: Hospital-scale chest x-ray database and benchmarks on weakly-supervised classification and localization of common thorax diseases. In *Proceedings of the IEEE conference on computer vision and pattern recognition*, pages 2097–2106, 2017.
- Pranav Rajpurkar, Jeremy Irvin, Kaylie Zhu, Brandon Yang, Hershel Mehta, Tony Duan, Daisy Ding, Aarti Bagul, Curtis Langlotz, Katie Shpanskaya, et al. Chexnet: Radiologist-level pneumonia detection on chest x-rays with deep learning. *arXiv preprint arXiv:1711.05225*, 2017.
- Qilong Wang, Banggu Wu, Pengfei Zhu, Peihua Li, Wangmeng Zuo, and Qinghua Hu. Eca-net: Efficient channel attention for deep convolutional neural networks. In *2020 IEEE/CVF Conference on Computer Vision and Pattern Recognition (CVPR)*, pages 11531–11539, 2020. doi:10.1109/CVPR42600.2020.01155.
- Tsung-Yi Lin, Piotr Dollár, Ross Girshick, Kaiming He, Bharath Hariharan, and Serge Belongie. Feature pyramid networks for object detection. In *2017 IEEE Conference on Computer Vision and Pattern Recognition (CVPR)*, pages 936–944, 2017. doi:10.1109/CVPR.2017.106.
- Karthik Ramamurthy, Illakiya Thayumanaswamy, Menaka Radhakrishnan, Daehan Won, and Sindhia Lingaswamy. Integration of localized, contextual, and hierarchical features in deep learning for improved skin lesion classification. *Diagnostics*, 14(13):1338, 2024.
- Ozan Oktay, Jo Schlemper, Loic Le Folgoc, Matthew Lee, Matthias Heinrich, Kazunari Misawa, Kensaku Mori, Steven McDonagh, Nils Y Hammerla, Bernhard Kainz, et al. Attention u-net: Learning where to look for the pancreas. *arXiv preprint arXiv:1804.03999*, 2018.
- Yan Liu, Yan Yang, Yongquan Jiang, and Zhuyang Xie. Multi-view orientational attention network combining point-based affinity for polyp segmentation. *Expert Systems with Applications*, 249:123663, 2024.
- Guimin Hou, Jiaohua Qin, Xuyu Xiang, Yun Tan, and Neal N Xiong. Af-net: A medical image segmentation network based on attention mechanism and feature fusion. *Computers, Materials & Continua*, 69(2):1877–1891, 2021.
- Jianwei Zheng, Hao Liu, Yuchao Feng, Jinshan Xu, and Liang Zhao. Casf-net: Cross-attention and cross-scale fusion network for medical image segmentation. *Computer Methods and Programs in Biomedicine*, 229:107307, 2023.
- Jeya Maria Jose Valanarasu, Poojan Oza, Ilker Hacihaliloglu, and Vishal M Patel. Medical transformer: Gated axial-attention for medical image segmentation. In *Medical image computing and computer assisted intervention—MICCAI 2021: 24th international conference, Strasbourg, France, September 27–October 1, 2021, proceedings, part I 24*, pages 36–46. Springer, 2021.

- Jiangyun Li, Wenxuan Wang, Chen Chen, Tianxiang Zhang, Sen Zha, Jing Wang, and Hong Yu. Towards better and more efficient volumetric segmentation of medical images. *arXiv preprint arXiv:2201.12785*, 2022.
- Yifan Jiang, Shiyu Chang, and Zhangyang Wang. Transgan: Two pure transformers can make one strong gan, and that can scale up. *Advances in Neural Information Processing Systems*, 34:14745–14758, 2021.
- Gorkem Can Ates, Prasoon Mohan, and Emrah Celik. Dual cross-attention for medical image segmentation. *Engineering Applications of Artificial Intelligence*, 126:107139, 2023.
- Xinrui Song, Hanqing Chao, Xuanang Xu, Hengtao Guo, Sheng Xu, Baris Turkbey, Bradford J Wood, Thomas Sanford, Ge Wang, and Pingkun Yan. Cross-modal attention for multi-modal image registration. *Medical Image Analysis*, 82:102612, 2022.
- Tao Wang, Xiumei Chen, Xiaoling Zhang, Shuoling Zhou, Qianjin Feng, and Meiyang Huang. Multi-view imputation and cross-attention network based on incomplete longitudinal and multimodal data for conversion prediction of mild cognitive impairment. *Expert Systems with Applications*, 231:120761, 2023a.
- Erico Tjoa and Cuntai Guan. A survey on explainable artificial intelligence (xai): Toward medical xai. *IEEE transactions on neural networks and learning systems*, 32(11):4793–4813, 2020.
- Edmon Begoli, Tanmoy Bhattacharya, and Dimitri Kuznetsov. The need for uncertainty quantification in machine-assisted medical decision making. *Nature Machine Intelligence*, 1(1):20–23, 2019.
- Shahriar Faghani, Mana Moassefi, Pouria Rouzrokh, Bardia Khosravi, Francis I Baffour, Michael D Ringle, and Bradley J Erickson. Quantifying uncertainty in deep learning of radiologic images. *Radiology*, 308(2):e222217, 2023.
- Ling Huang, Su Ruan, Yucheng Xing, and Mengling Feng. A review of uncertainty quantification in medical image analysis: Probabilistic and non-probabilistic methods. *Medical Image Analysis*, page 103223, 2024.
- Haoyuan Chen, Chen Li, Ge Wang, Xiaoyan Li, Md Mamunur Rahaman, Hongzan Sun, Weiming Hu, Yixin Li, Wanli Liu, Changhao Sun, et al. Gashis-transformer: A multi-scale visual transformer approach for gastric histopathological image detection. *Pattern Recognition*, 130:108827, 2022.
- Yundong Zhang, Huiye Liu, and Qiang Hu. Transfuse: Fusing transformers and cnns for medical image segmentation. In *Medical image computing and computer assisted intervention—MICCAI 2021: 24th international conference, Strasbourg, France, September 27–October 1, 2021, proceedings, Part I 24*, pages 14–24. Springer, 2021.
- Jutika Borah, Hidam Kumarjit Singh, and Kumaresh Sarmah. A deep ensemble approach for lung disease classification in chest x-ray across data distribution shifts and unseen data generalization. *SN Computer Science*, 5(7):835, 2024a.
- Benjamin Fritz, H Yi Paul, Richard Kijowski, and Jan Fritz. Radiomics and deep learning for disease detection in musculoskeletal radiology: an overview of novel mri-and ct-based approaches. *Investigative radiology*, 58(1):3–13, 2023.
- Jutika Borah, Hidam Kumarjit Singh, and Kumaresh Sarmah. Lung disease classification in chest x-rays with feature fusion via stacked convolutional denoising autoencoders. In *2023 IEEE International Conference on Computer Vision and Machine Intelligence (CVMI)*, pages 1–6. IEEE, 2023.
- Alhassan Ali Ahmed, Mohamed Abouzid, and Elzbieta Kaczmarek. Deep learning approaches in histopathology. *Cancers*, 14(21):5264, 2022.
- Michaela Unger and Jakob Nikolas Kather. Deep learning in cancer genomics and histopathology. *Genome medicine*, 16(1):44, 2024.
- Kai Jin and Juan Ye. Artificial intelligence and deep learning in ophthalmology: current status and future perspectives. *Advances in ophthalmology practice and research*, 2(3):100078, 2022.
- Kutubuddin SayyadLiyakat Kazi. Computer-aided diagnosis in ophthalmology: A technical review of deep learning applications. *Transformative Approaches to Patient Literacy and Healthcare Innovation*, pages 112–135, 2024.
- Jutika Borah, Kumaresh Sarmah, and Hidam Kumarjit Singh. Disease classification and impact of pretrained deep convolution neural networks on diverse medical imaging datasets across imaging modalities. *arXiv preprint arXiv:2408.17011*, 2024b.
- Vaswani Ashish. Attention is all you need. *Advances in neural information processing systems*, 30:I, 2017.

- Jieneng Chen, Jieru Mei, Xianhang Li, Yongyi Lu, Qihang Yu, Qingyue Wei, Xiangde Luo, Yutong Xie, Ehsan Adeli, Yan Wang, et al. Transunet: Rethinking the u-net architecture design for medical image segmentation through the lens of transformers. *Medical Image Analysis*, 97:103280, 2024.
- Dongxu Cheng, Zifang Zhou, and Jingwen Zhang. Eg-unetr: An edge-guided liver tumor segmentation network based on cross-level interactive transformer. *Biomedical Signal Processing and Control*, 97:106739, 2024.
- Jie Hu, Li Shen, and Gang Sun. Squeeze-and-excitation networks. In *Proceedings of the IEEE conference on computer vision and pattern recognition*, pages 7132–7141, 2018.
- Long Chen, Hanwang Zhang, Jun Xiao, Liqiang Nie, Jian Shao, Wei Liu, and Tat-Seng Chua. Sca-cnn: Spatial and channel-wise attention in convolutional networks for image captioning. In *Proceedings of the IEEE conference on computer vision and pattern recognition*, pages 5659–5667, 2017.
- Sanghyun Woo, Jongchan Park, Joon-Young Lee, and In So Kweon. Cbam: Convolutional block attention module. In *Proceedings of the European conference on computer vision (ECCV)*, pages 3–19, 2018.
- Jifeng Dai, Haozhi Qi, Yuwen Xiong, Yi Li, Guodong Zhang, Han Hu, and Yichen Wei. Deformable convolutional networks. In *Proceedings of the IEEE international conference on computer vision*, pages 764–773, 2017.
- Hengshuang Zhao, Jiaya Jia, and Vladlen Koltun. Exploring self-attention for image recognition. In *Proceedings of the IEEE/CVF conference on computer vision and pattern recognition*, pages 10076–10085, 2020.
- Keya Wang, Chuanyun Xu, Gang Li, Yang Zhang, Yu Zheng, and Chengjie Sun. Combining convolutional neural networks and self-attention for fundus diseases identification. *Scientific Reports*, 13(1):76, 2023b.
- Ze Liu, Yutong Lin, Yue Cao, Han Hu, Yixuan Wei, Zheng Zhang, Stephen Lin, and Baining Guo. Swin transformer: Hierarchical vision transformer using shifted windows. In *Proceedings of the IEEE/CVF international conference on computer vision*, pages 10012–10022, 2021.
- Jianwei Yang, Chunyuan Li, Pengchuan Zhang, Xiyang Dai, Bin Xiao, Lu Yuan, and Jianfeng Gao. Focal self-attention for local-global interactions in vision transformers. *arXiv preprint arXiv:2107.00641*, 2021.
- Yuhui Yuan, Rao Fu, Lang Huang, Weihong Lin, Chao Zhang, Xilin Chen, and Jingdong Wang. Hrformer: High-resolution vision transformer for dense predict. *Advances in neural information processing systems*, 34: 7281–7293, 2021.
- Jo Schlemper, Ozan Oktay, Michiel Schaap, Mattias Heinrich, Bernhard Kainz, Ben Glocker, and Daniel Rueckert. Attention gated networks: Learning to leverage salient regions in medical images. *Medical image analysis*, 53: 197–207, 2019.
- Qingji Guan, Yaping Huang, Zhun Zhong, Zhedong Zheng, Liang Zheng, and Yi Yang. Thorax disease classification with attention guided convolutional neural network. *Pattern Recognition Letters*, 131:38–45, 2020.
- Abdur R Fayjie, Jutika Borah, Florencia Carbone, Jan Tack, and Patrick Vandewalle. Predictive uncertainty estimation in deep learning for lung carcinoma classification in digital pathology under real dataset shifts. *arXiv preprint arXiv:2408.08432*, 2024.
- Xin Bai, Zhengyu Jin, and Hao Sun. Can uncertainty quantification of ai prediction models benefit young radiologists more? *Radiology*, 310(2):e232781, 2024.
- Ke Zou, Zhihao Chen, Xuedong Yuan, Xiaojing Shen, Meng Wang, and Huazhu Fu. A review of uncertainty estimation and its application in medical imaging. *Meta-Radiology*, 1(1):100003, 2023.
- Jakob Gawlikowski, Cedrique Rovile Njiteucheu Tassi, Mohsin Ali, Jongseok Lee, Matthias Humt, Jianxiang Feng, Anna Kruspe, Rudolph Triebel, Peter Jung, Ribana Roscher, et al. A survey of uncertainty in deep neural networks. *Artificial Intelligence Review*, 56(Suppl 1):1513–1589, 2023.
- Alex Kendall and Yarin Gal. What uncertainties do we need in bayesian deep learning for computer vision? *Advances in neural information processing systems*, 30, 2017.
- Tanya Nair, Doina Precup, Douglas L Arnold, and Tal Arbel. Exploring uncertainty measures in deep networks for multiple sclerosis lesion detection and segmentation. *Medical image analysis*, 59:101557, 2020.
- Paulo Chagas, Luiz Souza, Izabelle Pontes, Rodrigo Calumby, Michele Angelo, Angelo Duarte, Washington Lc-Dos Santos, and Luciano Oliveira. Uncertainty-aware membranous nephropathy classification: A monte-carlo dropout approach to detect how certain is the model. *Computer Methods in Biomechanics and Biomedical Engineering: Imaging & Visualization*, 11(3):288–298, 2023.
- Thomas-Martin Dutschmann, Lennart Kinzel, Antonius Ter Laak, and Knut Baumann. Large-scale evaluation of k-fold cross-validation ensembles for uncertainty estimation. *Journal of cheminformatics*, 15(1):49, 2023.

- Muhammad EH Chowdhury, Tawsifur Rahman, Amith Khandakar, Rashid Mazhar, Muhammad Abdul Kadir, Zaid Bin Mahbub, Khandakar Reajul Islam, Muhammad Salman Khan, Atif Iqbal, Nasser Al Emadi, et al. Can ai help in screening viral and covid-19 pneumonia? *Ieee Access*, 8:132665–132676, 2020.
- Tawsifur Rahman, Amith Khandakar, Muhammad Abdul Kadir, Khandaker Reajul Islam, Khandakar F Islam, Rashid Mazhar, Tahir Hamid, Mohammad Tariqul Islam, Saad Kashem, Zaid Bin Mahbub, et al. Reliable tuberculosis detection using chest x-ray with deep learning, segmentation and visualization. *Ieee Access*, 8: 191586–191601, 2020.
- Daniel Kermany. Labeled optical coherence tomography (oct) and chest x-ray images for classification. *Mendeley data*, 2018.
- Mingxing Tan and Quoc Le. Efficientnet: Rethinking model scaling for convolutional neural networks. In *International conference on machine learning*, pages 6105–6114. PMLR, 2019.
- Kaiming He, Xiangyu Zhang, Shaoqing Ren, and Jian Sun. Deep residual learning for image recognition. In *Proceedings of the IEEE conference on computer vision and pattern recognition*, pages 770–778, 2016.
- Jingyao Li, Lianglun Cheng, Tingjian Xia, Haomin Ni, and Jiao Li. Multi-scale fusion u-net for the segmentation of breast lesions. *IEEE Access*, 9:137125–137139, 2021.
- Mengqi Xu, Qianting Ma, Huajie Zhang, Dexing Kong, and Tiejong Zeng. Mef-unet: An end-to-end ultrasound image segmentation algorithm based on multi-scale feature extraction and fusion. *Computerized Medical Imaging and Graphics*, 114:102370, 2024.
- Xiangzuo Huo, Gang Sun, Shengwei Tian, Yan Wang, Long Yu, Jun Long, Wendong Zhang, and Aolun Li. Hifuse: Hierarchical multi-scale feature fusion network for medical image classification. *Biomedical Signal Processing and Control*, 87:105534, 2024.
- Along He, Tao Li, Ning Li, Kai Wang, and Huazhu Fu. Cabnet: Category attention block for imbalanced diabetic retinopathy grading. *IEEE Transactions on Medical Imaging*, 40(1):143–153, 2020.
- Xiaomeng Li, Xiaowei Hu, Lequan Yu, Lei Zhu, Chi-Wing Fu, and Pheng-Ann Heng. Canet: cross-disease attention network for joint diabetic retinopathy and diabetic macular edema grading. *IEEE transactions on medical imaging*, 39(5):1483–1493, 2019.
- Hai Xie, Xianlu Zeng, Haijun Lei, Jie Du, Jiantao Wang, Guoming Zhang, Jiuwen Cao, Tianfu Wang, and Baiying Lei. Cross-attention multi-branch network for fundus diseases classification using slo images. *Medical Image Analysis*, 71:102031, 2021.
- Yarin Gal and Zoubin Ghahramani. Dropout as a bayesian approximation: Representing model uncertainty in deep learning. In *international conference on machine learning*, pages 1050–1059. PMLR, 2016.
- Claude Elwood Shannon. A mathematical theory of communication. *The Bell system technical journal*, 27(3): 379–423, 1948.
- Moloud Abdar, Mohammad Amin Fahami, Satarupa Chakrabarti, Abbas Khosravi, Paweł Pławiak, U Rajendra Acharya, Ryszard Tadeusiewicz, and Saeid Nahavandi. Barf: A new direct and cross-based binary residual feature fusion with uncertainty-aware module for medical image classification. *Information Sciences*, 577: 353–378, 2021.
- Jiancheng Yang, Rui Shi, Donglai Wei, Zequan Liu, Lin Zhao, Bilian Ke, Hanspeter Pfister, and Bingbing Ni. Medmnist v2-a large-scale lightweight benchmark for 2d and 3d biomedical image classification. *Scientific Data*, 10(1):41, 2023.
- Prateek Chhikara, Prabhjot Singh, Prakhhar Gupta, and Tarunpreet Bhatia. Deep convolutional neural network with transfer learning for detecting pneumonia on chest x-rays. In *Advances in Bioinformatics, Multimedia, and Electronics Circuits and Signals: Proceedings of GUCON 2019*, pages 155–168. Springer, 2020.